Cutoff Size Need Not Strongly Influence Molecular Dynamics Results for Solvated Polypeptides†

David A. C. Beck,‡ Roger S. Armen,‡ and Valerie Daggett*,‡,§

Biomolecular Structure and Design Program, University of Washington, Seattle, Washington 98195-7610, and Department of Medicinal Chemistry, University of Washington, Seattle, Washington 98195-7610

Received June 29, 2004; Revised Manuscript Received October 26, 2004

ABSTRACT: The correct treatment of van der Waals and electrostatic nonbonded interactions in molecular force fields is essential for performing realistic molecular dynamics (MD) simulations of solvated polypeptides. The most computationally tractable treatment of nonbonded interactions in MD utilizes a spherical distance cutoff (typically, 8−12 Å) to reduce the number of pairwise interactions. In this work, we assess three spherical atom-based cutoff approaches for use with all-atom explicit solvent MD: abrupt truncation, a CHARMM-style electrostatic shift truncation, and our own force-shifted truncation. The chosen system for this study is an end-capped 17-residue alanine-based α-helical peptide, selected because of its use in previous computational and experimental studies. We compare the time-averaged helical content calculated from these MD trajectories with experiment. We also examine the effect of varying the cutoff treatment and distance on energy conservation. We find that the abrupt truncation approach is pathological in its inability to conserve energy. The CHARMM-style shift truncation performs quite well but suffers from energetic instability. On the other hand, the force-shifted spherical cutoff method conserves energy, correctly predicts the experimental helical content, and shows convergence in simulation statistics as the cutoff is increased. This work demonstrates that by using proper and rigorous techniques, it is possible to correctly model polypeptide dynamics in solution with a spherical cutoff. The inherent computational advantage of spherical cutoffs over Ewald summation (and related) techniques is essential in accessing longer MD time scales.

Accurate molecular dynamics (MD)[1] simulations of polypeptides in solution necessitate robust methodologies. The selection of certain methodologies, such as the use of all-atom molecular mechanics potentials and explicit representation of fully flexible waters, is important for obtaining correct, experimentally verifiable results (*1*). However, some aspects, such as the choice of treatments for the nonbonded atomic interactions, are up for debate (*2*−*9*). As such, it is important that they be continually re-examined and carefully tested against experiment. Furthermore, MD simulations using force fields originally derived from, and parametrized against, static states (i.e., crystal structures) must be evaluated against experiments that reflect the dynamic properties of a system.

As computer power increases, it is necessary to continually test and evaluate MD methods using successively longer simulations (*10*). These methods should be tested for stability (e.g., conservation of conserved properties), accuracy (e.g., proper treatment of short- and long-range forces), and completeness (i.e., conformational sampling). For these purposes, peptides that are well characterized by circular dichroism (CD) and solution nuclear magnetic resonance (NMR) spectroscopy are useful systems for testing the accuracy of these methods against the respective ensemble-averaged experimental observables. Further, because of their small size, explicitly solvated peptide systems are computationally less expensive than identically treated proteins. The inherently dynamic nature of peptides provides a good test of the sampling capabilities of MD. For example, within the time scale of the molecular dynamics trajectory, are the experimentally averaged data (e.g., from both "folded" and "unfolded" conformations) adequately reproduced?

In this work, we use robust MD methods (*1*) to evaluate the stability, accuracy, and completeness of several spherical cutoff treatments. Previous tests for accurate treatment of long-range electrostatic interactions in alanine-based helical peptides have used the stability of the α-helix as the primary criterion for correct treatment of interactions (*4*−*6*). For example, in a highly cited paper, Schreiber and Steinhauser (*4*) focused on the $Y(KAAAA)_3K\text{-}NH_2$ peptide (*11*) and compared simulations computed using an abrupt group-based truncation, with 6, 10, and 14 Å spherical cutoffs for the nonbonded interactions, with simulations calculated using Ewald summations. The simulations they performed were as short as 60 ps and as long as 825 ps; all were conducted at 300 K. They observed a lack of convergence of the helical content (derived primarily from visual inspection of struc-

† This work was supported by the National Institutes of Health (Grant GM 50789 to V.D.). D.A.C.B. and R.S.A. were supported by an NIH Molecular Biophysics Training Grant (National Research Service Award 5 T32 GM 08268).

* To whom correspondence should be addressed. E-mail: daggett@u.washington.edu.

‡ Biomolecular Structure and Design Program.

§ Department of Medicinal Chemistry.

[1] Abbreviations: MD, molecular dynamics; CD, circular dichroism; NMR, nuclear magnetic resonance; PME, particle mesh Ewald; NVE, constant number of particles, volume, and energy; *il*mm, *in lucem* Molecular Mechanics; NVE*p*, constant number of particles, volume, energy, and linear momentum; rmsd, root-mean-square deviation.

10.1021/bi0486381 CCC: $30.25
Published on Web 12/18/2004

tures) for the different cutoffs. Further, their simulation employing Ewald sum (*12*) calculations produced a very stable α-helix unlike the abrupt cutoff simulations, which sampled both nonhelical and partially helical structures. Almost solely on the basis of these findings, they concluded that MD simulations are heavily perturbed by truncation and are therefore unreliable. However, the experimental helical content is approximately 50% at 300 K, as estimated by the method of Chakrabartty et al. using the experimental value of 78% at 273 K (*11*, *13*). In this regard, Schreiber and Steinhauser's Ewald simulation is inconsistent with experiment and predicts a helix content much higher than the observed content.

Despite the fact that Schreiber and Steinhauser's study utilized only simple, abrupt truncation, it has been taken as proof by some that all spherical cutoff methods are incapable of providing stable and accurate simulations. This misinterpretation has been carried so far that some insist that Ewald summations are required, instead of cutoff schemes, for realistic simulations. To dispel the misconception that all spherical cutoffs are similarly deficient for simulation of biomolecules, it is important to distinguish between different spherical cutoff treatments. Here we present the results of MD simulations of the same peptide investigated by Schreiber and Steinhauser using abrupt truncation and two different shifting truncation methods. A force shift method we call "ours" is used in ENCAD (*8*) and in *in lucem* Molecular Mechanics (*il*mm, D. A. C, Beck, D. O. V. Alonso, and V. Daggett, University of Washington), and the other is a shift method commonly employed in CHARMM (*9*, *14*). The simulations are 1−2 orders of magnitude longer than the earlier Schreiber and Steinhauser simulations to ensure that we have adequate sampling. Contrary to Schreiber and Steinhauser's study, we find that similar results are obtained with our force-shifted cutoff method using 8, 10, 12, 14, and 16 Å cutoffs. That is, they converge as the cutoff range is increased beyond 8 Å; furthermore, the results are in agreement with experiment.

MATERIALS AND METHODS

Nonbonded Spherical Cutoff Methods. In all-atom MD simulations of macromolecules in solution, it is neither possible nor necessary to evaluate all of the pairwise nonbonded interactions arising from an infinite solution, as a periodic box might suggest. In general, two common approaches to dealing with this problem are used: spherical cutoffs (*7*, *9*) and Ewald summation (*12*), both traditional and PME (*15*, *16*). With spherical cutoffs, the favored method of balancing the resulting foreshortened nonbonded potential is dubbed force shifting (*7*, *8*). An alternative is abrupt truncation, which from first principles will affect the integrity of the simulation (*7*). In addition, not all spherical cutoff approaches modify both the electrostatic and the van der Waals portions of the original nonbonded potential, $U_{nb,0}$.

Equation 1 describes simple truncation. Beyond the spherical cutoff distance, or R_c, the energy of interaction is zero; no attempt is made to smoothly drive the energy to zero by the cutoff. This approach is the simplest and most problematic, and it was the method employed by Schreiber and Steinhauser. With such abrupt truncation, energy is not conserved, and therefore, simulations in the NVE (microcanonical) ensemble rescale frequently.

$$U_{nb}(r) = \begin{cases} r < R_c \rightarrow U_{nb,0}(r) \\ r \geq R_c \rightarrow 0 \end{cases} \quad (1)$$

A more correct cutoff approach is force shifting. Fundamentally, this involves driving $U_{nb,0}$ to zero by R_c and thus conserving energy at the expense of slightly modifying the pairwise interaction energy. The method we use, hereafter termed our method (in eq 2), subtracts the first-order Taylor series expansion of $U_{nb,0}$ about R_c from $U_{nb,0}$ (*8*). This has the effect of preserving the energies as much as possible with only very small changes to the forces.

$$U_{nb}(r) = \begin{cases} r < R_c \rightarrow U_{nb,0}(r) - \left[U_{nb,0}(R_c) + (r - R_c)\left[\dfrac{dU_{nb,0}(R_c)}{dr}\right]\right] \\ r \geq R_c \rightarrow 0 \end{cases} \quad (2)$$

CHARMM (*9*, *14*) uses a similar approach for the electrostatics (eq 3) but simply truncates the van der Waals interactions (which is less problematic than sharp truncation of the electrostatic terms). However, this scheme can lead to distortion of hydrogen bond linearity (*8*). Nevertheless, this approach is vastly superior to eq 1.

$$U_{nb}(r) = \begin{cases} r \leq R_c \rightarrow U_{nb,0}(r)\left[1 - \left(\dfrac{r}{R_c}\right)^2\right]^2 \\ r > R_c \rightarrow 0 \end{cases} \quad (3)$$

The choice of R_c is not arbitrary. Longer cutoffs are always desirable, but given the very real constraints on computer time and the need for extensive sampling to realistically model protein conformational behavior, we have taken a pragmatic stance and opted for better sampling. Thus, we typically employ nonbonded spherical cutoff radii of 8, 10, and occasionally 12 Å. In addition, we note that the standard deviation of the mean varies as $1/n^2$ (*17*) such that longer simulations can provide more precise results, not to mention that the process of interest may not even be observed in a shorter simulation.

Molecular Dynamics Simulations. To assess the convergence of these three spherical cutoff approaches, we have performed MD simulations of the same peptide studied by Schreiber and Steinhauser [Ac-Y$(KAAAA)_3$K-NH_2 (*11*)]. These MD simulations were conducted with a range of spherical cutoff treatments and radii. A summary of the simulations performed is presented in Table 1. The simulations were performed using *il*mm with explicit F3C (*18*) waters and all hydrogens at 298 K using protocols described in detail elsewhere (*1*). The nonbonded interaction pair lists were updated every three steps. All simulations were 11 ns long with the last 10 ns used for analysis. Simulations A−F used our force-shifting method with 6, 8, 10, 12, 14, and 16 Å spherical cutoff values, respectively. The peptide was solvated in a box extending at least 16 Å from any solute atom, with edge dimensions of 63.45 Å × 46.75 Å × 45.24 Å, hereafter termed the 16 Å box. To demonstrate that convergence of helical properties is not box size-dependent, additional simulations with smaller 8 and 10 Å boxes (with dimensions of 30.77 Å × 47.50 Å × 29.24 Å and 51.48 Å

Table 1: Summary of $Y(KAAAA)_3K\text{-}NH_2$ Peptide MD Runs with Various Spherical Cutoff Treatments

identifier[a]	spherical cutoff range (Å)	spherical cutoff treatment	solvation box depth (Å)	helix content[b] (%)	energy drift per nanosecond[c] (%)	no. of velocity rescales in the final 10 ns[d]
A	6	force shift	16	9 ± 6	0.344	7
B	8	force shift	16	59 ± 18	0.112	2
C	10	force shift	16	63 ± 13	0.054	1
D	12	force shift	16	58 ± 12	0.038	0
E	14	force shift	16	63 ± 13	0.029	0
F	16	force shift	16	63 ± 14	0.024	0
G	6	abrupt	16	20 ± 16	441	5×10^4
H	8	abrupt	16	70 ± 12	246	5×10^4
I	10	abrupt	16	54 ± 14	170	2.8×10^4
J	12	abrupt	16	40 ± 13	123	2.5×10^4
K	14	abrupt	16	32 ± 15	108	1.8×10^4
L	16	abrupt	16	28 ± 13	94.6	1.3×10^4
M	6	CHARMM	16	14 ± 15	10.1	231
N	8	CHARMM	16	35 ± 16	4.82	118
O	10	CHARMM	16	52 ± 14	1.71	51
P	12	CHARMM	16	45 ± 12	1.04	18
Q	14	CHARMM	16	40 ± 12	0.812	20
R	16	CHARMM	16	36 ± 13	0.630	12
S	8	force shift	10	54 ± 12	0.114	2
T	10	force shift	10	58 ± 14	0.063	2
U	8	abrupt	10	13 ± 21	315	5×10^4
V	10	abrupt	10	20 ± 18	186	3.01×10^4
X	8	CHARMM	10	34 ± 15	5.02	159
Y	10	CHARMM	10	45 ± 12	2.11	73
Z	8	force shift	8	54 ± 14	0.201	3
AA	8	abrupt	8	10 ± 24	228	5×10^4
AB	8	CHARMM	8	37 ± 14	5.13	148

[a] W was intentionally omitted. [b] Helix content statistics were calculated with the method of Pardi et al. (*19*) for the last 10 ns of each 298 K simulation. [c] Drift of total energy in percent for the final nanosecond derived from a linear fit of the data. In cases where the simulation rescaled during the final nanosecond, the largest intermediate time regime between rescales was fit and extrapolated for drift over 1 ns. [d] The raw number of energy rescalings over the final 10 ns of the 11 ns simulation.

× 34.76 Å × 33.24 Å, respectively) were performed (S, T, and Z). To compare our force shifting method to the CHARMM (*14*) method (eq 3), simulations M−R using the CHARMM-style shift in an 16 Å box were also performed as well as additional similar simulations in smaller boxes (X, Y, and AB). Finally, to mimic the Schreiber and Steinhauser setup, simulations G−L were conducted using abrupt truncation in a 16 Å box as well as additional similar simulations in smaller boxes (U, V, and AA), although we note that their boxes were much smaller.

Analysis of Helical Content. The mean and standard deviation of the helical content (over the last 10 ns) of each simulation was evaluated according to the method of Pardi et al. (*19*), which weights longer helical segments more heavily than short ones. This method for evaluation of helix content is commonly used in other studies of alanine-based helical peptides (*20*, *21*) and was originally parametrized against globular proteins (*19*). The Pardi method can slightly overestimate the helical percentage when compared to the value derived from CD experiments by as much as 10%. However, we note that other definitions give comparable relative results. Structures for this analysis were sampled from the 10 ns thermally equilibrated ensemble at 1 ps intervals, yielding 10 000 samples for each simulation.

RESULTS

The summary statistics for the simulations can be found in Table 1, and snapshots taken from each of the simulations can be found in Figure 1. For reference, the helical content derived from CD is approximately 50% at 298 K (*11*, *13*). Figure 2 illustrates the effect of cutoff radius and spherical cutoff treatment on the helical content. To demonstrate how two popular force-shifted cutoff ranges sample an ensemble of both nonhelical and helical conformations, Figure 3 presents snapshots from simulations B and C. The snapshots in Figure 3 contain helical contents from the low and high tails of the helical content distribution as well as its mean (∼50%). Figure 3 shows that unlike Schreiber and Steinhauser's Ewald simulations that never diverged from highly helical conformers, our force shift method sampled both helical and nonhelical states.

It is clear from the very low helical content (9 ± 6%) that the 6 Å force shift cutoff (simulation A) failed to accurately model the nonbonded interactions, thereby failing to represent the gross structural properties of the peptide. In contrast, when the force shift spherical cutoff is extended to ≥8 Å (simulations B−F, S, T, and Z), the helical content converged with means between 54 and 63, which are in agreement with experiment. The subset of force shift trajectories B−F, all of which used a 16 Å water box (at least 16 Å between any peptide atom and the edge of the box), yielded helix contents similar to those obtained with 8 (Z) and 10 Å water boxes (S and T). Simulations T and Z were continued to 51 ns, and the helical content was calculated for the last 10 ns. These contents of 56 ± 11 and 54 ± 14%, respectively, are in good agreement with the 1−11 ns means for these simulations (58 ± 14 and 52 ± 12%, respectively), indicating convergence in this property on the shorter time scale.

The CHARMM-style simulations (M−R, X, Y, and AB) yielded mean helical contents ranging from 14 to 45%. Most of these simulations have average values that are too low, but most are in agreement with experiment if the standard

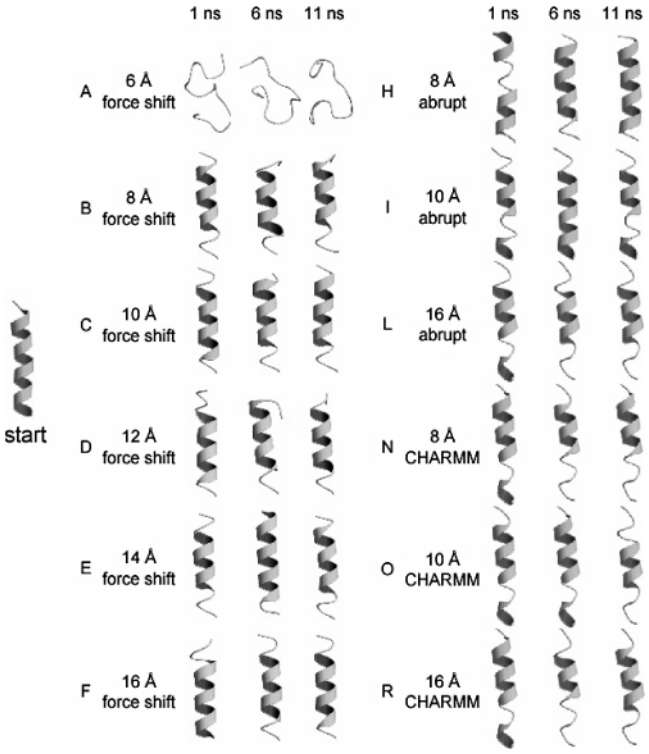

FIGURE 1: Snapshots of $Y(KAAAA)_3K\text{-}NH_2$ peptide MD runs with various spherical cutoff treatments. The simulation identifiers (A−F, T, Z, AA, and AB) match those from Table 1. At the left is the all-helical conformation used to start all the simulations. For each simulation, three snapshots are shown corresponding to 1, 6, and 11 ns. All structures are best fit to the starting structure and oriented with the N-terminus at the bottom. Regions that are predicted ($P > 0.90$, i.e., four or more consecutive residues for which $J_{H\alpha N} < 6.0$ Hz) to be helical by the method of Pardi et al. (*19*) are drawn with ribbons. Hydrogens, side chains, and waters that are included in the simulation calculations have been removed for clarity.

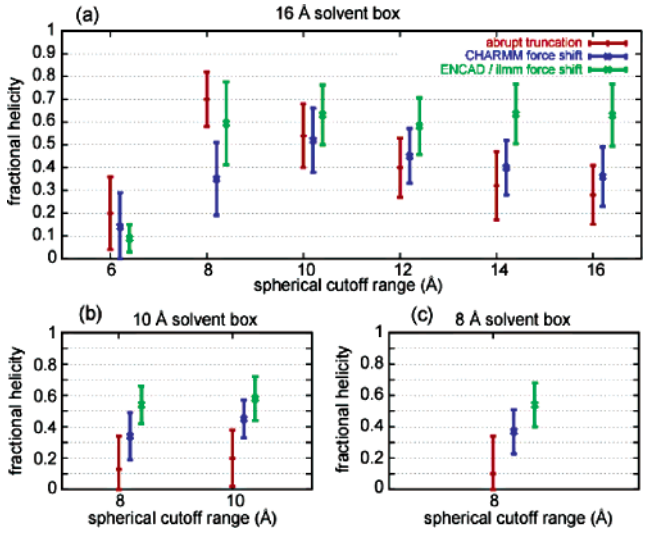

FIGURE 2: Peptide $Y(KAAAA)_3K\text{-}NH_2$ fraction helix determined by the method of Pardi et al. (*19*) derived from MD runs with various spherical cutoff treatments and explicit solvent depths. Values with error bars (of one standard deviation) are shown for three spherical cutoff treatments: abrupt truncation (red), a CHARMM-style force shift applied to electrostatics only (blue), and our atom force shift (green). In panel a, simulations were conducted in an explicit solvent extending at least 16 Å from any peptide atom. To demonstrate that these values are not sensitive to solvent depth (i.e., periodic box size), panels b and c depict the fractional helical content for simulations conducted with solvent depths of 10 and 8 Å, respectively.

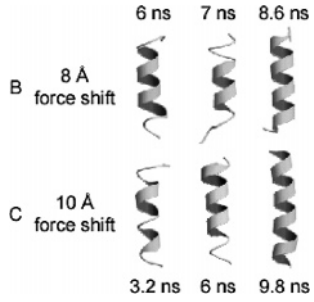

FIGURE 3: Snapshots of $Y(KAAAA)_3K\text{-}NH_2$ peptide MD runs illustrating dynamic helical content. The simulation identifiers (B and C) match those from Table 1. For each simulation, three snapshots are presented with the indicated time. All structures are best fit to the starting structure and oriented with the N-terminus at the bottom. Regions that are predicted ($P > 0.90$, i.e., four or more consecutive residues for which $J_{H\alpha N} < 6.0$ Hz) to be helical by the method of Pardi et al. (*19*) are drawn with ribbons. Hydrogens, side chains, and waters that are included in the simulation calculations have been removed for clarity.

deviations are included. However, these simulations were less energetically stable, and therefore, the velocities required more frequent rescaling than the convergent force shift simulations (Table 1). Examination of the peptide structures in Figure 1 provides further insights: while the structures generated using the CHARMM cutoff scheme are not as disrupted as those in simulation A using a 6 Å cutoff, they are somewhat different from those presented for our force-shifted scheme (B−F, S, T, and Z). On average, for comparable cutoffs, the helix content was higher using our scheme than CHARMM's (59% vs 42%, Figure 2).

For both the CHARMM and abrupt truncation treatments, there is a maximum, in the helical content at 10 and 8 Å, respectively. Similar behavior was observed by Schreiber and Steinhauser for their abrupt truncation simulations; they attributed it to fortuitously choosing the correct cutoff radius for a given method. However, because at least for abrupt truncation, this trend is not observed when the box size is reduced, the idea of a "correct cutoff radius" for either of these methods is dubious. The discrepancy in behavior when the box size is changed (8 Å for simulations H, U, and AA and 10 Å for simulations I and V) is likely due to effectively increasing the volume of the energy fluctuation "damping bath" by adding more fully flexible waters to the simulation system. This can most clearly be seen by comparing the energy drift estimates and the number of rescalings for the 16 Å solvent box simulations versus the 10 and 8 Å solvent box simulations with the same cutoff (Table 1).

In the force-shifted simulations, the helical content was insensitive to changes in the cutoff from 8 to 16 Å (Figure 2a). Similarly, for a given cutoff, the results were independent of box size (Figure 2b,c). In addition, all of the simulations using our force-shifted procedure conserved energy, unlike the other methods (Table 1).

DISCUSSION

The similarity of the helical content for our force shift spherical cutoff simulations using 8, 10, 12, 14, and 16 Å cutoffs and the fact that the calculated helix content is in good agreement with experiment demonstrate that it is

possible to correctly model the nonbonded interactions in explicitly solvated polypeptide systems using spherical nonbonded cutoffs (Table 1). Of simulations B−F, only B and C rescaled after the 1 ns equilibration period. From this, it is clear that the energy drift was minor in all cases. Thus, the force shift treatment conserved energy and was numerically stable. Similarly, the helical contents calculated are in agreement with experiment. Furthermore, the helical content in simulations B−F is indistinguishable from that of identically treated systems in smaller solvent boxes (S, T, and Z).

From first principles, regardless of the ensemble, it is essential that a simulation conserve the ensemble's thermodynamic quantities. In our preferred ensemble, NVE*p*, the drift in total energy and the frequency of velocity rescalings provide feedback about the physical correctness of the simulation. For each of the simulations in Table 1, we present the energy drift over the final nanosecond (or extrapolations from the largest rescale-free region therein) as well as the number of velocity rescalings over the final 10 ns of the simulations. Our force shift approach produces very little drift, and we postulate that the 16 Å cutoff (simulation F) drift of 0.024% per nanosecond may be a realistic estimate of the lower bound imposed by numerical error (i.e., roundoff error) on a simulation of this size in *il*mm.

In the case of the abrupt cutoff simulations (G−L, U, V, and AA), it was not possible to conserve energy at any cutoff distance. The best drift was 94% per nanosecond for a simulation conducted with a 16 Å cutoff (L). In this case, there were more than 13 000 velocity rescalings over the final 10 ns of the simulation. Given the numerical instability of abrupt truncation simulations, the practical results confirm the first principles fact that abrupt truncation spherical cutoffs are problematic for solvated polypeptide MD simulations. However, one must keep in mind that cutoff treatments differ, as do the results one obtains with them. It is clearly wrong to assume that all cutoff methods are flawed, based on results obtained using just an abrupt cutoff.

Energy conservation for the CHARMM-style shift (simulations M−R, X, Y, and AB) is tightly linked to the cutoff distance. As the van der Waals component of the energy function is abruptly truncated in this approach, even at distances longer than 10 Å there are significant discontinuities at the cutoff to severely spoil energy conservation, resulting in a large number of rescalings (∼20). At long cutoffs (16 Å), the CHARMM shift reaches its maximum level of energy conservation at an ∼0.6% per nanosecond drift.

Numerical instability of the magnitude encountered when using abrupt cutoffs and to a lesser extent with the CHARMM-style truncation at short cutoff distances is problematic. Frequent energy rescaling can perturb the system in unpredictable ways (*22*) and also lead to discontinuous trajectories, which is a problem if one wants to map time-dependent processes or conformational changes. We note that while our implementation of a CHARMM-style shift is consistent with eq 3, *il*mm uses a different force field and subsequently different parameters. Consequently, we may not precisely duplicate CHARMM's (i.e., the software's) polypeptide dynamics.

Most investigators do not report variances in the conserved thermodynamic variables (e.g., in our case energy), and instead, for native state simulations of proteins, they use structural stability alone (i.e., C_α rmsd from the crystal structure) as a means of evaluating the accuracy of their nonbonded treatments. This is an insufficient criterion for comparison. One can imagine the trivial case in which nonbonded interactions are treated as harmonic oscillators about their respective distances derived from the crystal. Such a treatment would satisfy the stability criterion, but would be of no significant scientific value. Rather, it is more appropriate to compare against multiple ensemble-averaged experimental properties of a dynamic system. To this end, we previously extended Schreiber and Steinhauser's study to a similar alanine-based peptide that has been characterized by CD and high-resolution NMR. In that study, we compared the results of different cutoffs to multiple ensemble-averaged experimental observables (*23*), and again we showed that our force-shifted cutoff method provided results in good agreement with experiment.

It should be noted that the Schreiber and Steinhauser simulations were significantly shorter than the 11 ns simulations presented here and comprised a time interval which we typically disregard in our work as "system equilibration". It is doubtful, however, that longer abrupt cutoff trajectories would have significantly altered their results: a physically incorrect simulation will always be incorrect, despite its length. Our simulations using an abrupt 8 Å cutoff were similarly misbehaved. They may have seen their Ewald trajectory diverge more from the starting helical state to a more experimentally agreeable distribution had they continued it, but at the time of their publication, computational resources severely limited sampling.

The Ewald summation method arises from work in the early part of the last century that desired to derive a solution for the electrostatic energies of ionic crystal lattices with low dielectric constants. In 1921, Ewald (*12*) transformed the infinite (conditionally convergent) triple sum of the Coulombic lattice sum, eq 1 of ref *15*, into two absolutely convergent sums, eq 2 of ref *15*. This mathematical transformation has absolutely no physical basis (*24*). However, it has been widely exploited for its original purpose (i.e., evaluating the electrostatic energies of crystal lattices) and dramatically different problems, including calculation of long-range electrostatics of proteins in water, decidedly nonperiodic, nonlattice, high-dielectric systems.

In the solution state, the extent and therefore the necessity of such long-range electrostatic interactions are debatable. Many assume, based on evidence from crystal lattices of ions, that these effects are very long range. However, experiments with ions in water, as well as proteins in solution, indicate that the effective field of charges is quite short and on the order of 8−12 Å. Essentially, the high relative permittivity of water ($\epsilon = 78$ at 298 K) effectively screens those charge−charge interactions at distances beyond typical R_c values for spherical cutoff approaches. In other words, the experimentally determined dielectric constant rises very steeply at short distances, as illustrated in Figure 4. For example, experimental studies of ions in water indicate that the dielectric constant is approximately 45 at 8 Å, increasing to 55 and 65 at 10 and 12 Å, respectively (*25*) (see the Conway curve in Figure 4).

Another common misconception is that the internal effective dielectric of proteins ranges from 2 to 4. This value is derived from experimental evaluation of protein dielectrics

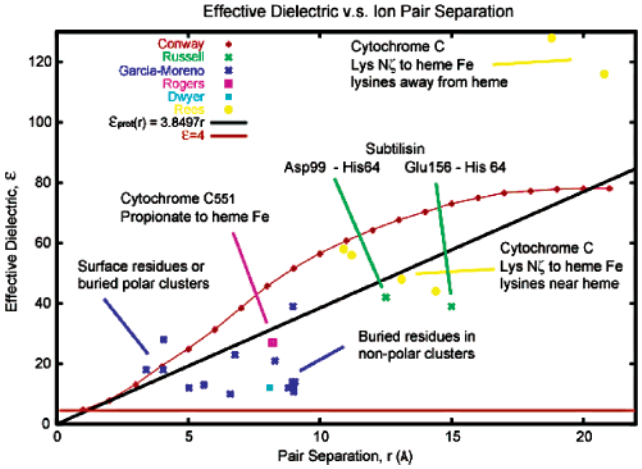

FIGURE 4: Effective dielectric as a function of increasing ion pair separation in water and proteins. The red points describe the effective dielectric for increasing pair separation in water [data from experimental work of Conway (*25*)]. Plotted in green are experimental protein apparent dielectric data from Russel et al. (*28*, *29*). In blue are plotted effective protein dielectrics from the experimental work of Garcia-Moreno (*31*). Similarly, in purple, cyan, and yellow are depicted experimental measurements of internal protein dielectrics by Rogers (*32*), Dwyer (*30*), and Rees (*27*), respectively. A linear best fit of the protein effective dielectric data is represented by the black line [$\epsilon_{prot}(r)$]. The equation for this fit is $\epsilon_{prot}(r) = 3.8497r$, with a correlation coefficient R of 0.77. The orange line represents the equality $\epsilon = 4$, which is a common approximation for the internal dielectric constant of a protein. Where possible, groups of points with similar characteristics have been labeled with colored lines linking the label and points of interest.

using dried, powdered proteins (*26*). In reality, for the solution state (the biologically relevant state), the dielectric constant of proteins is much closer to that of water than the commonly assumed value ($\epsilon = 2-4$). Experimental evaluations of true solution state internal protein effective dielectrics by pK_a shifts (*27*−*32*) have found dielectric constants on the order of ∼35 at 10 Å and ∼50 at 15 Å (Figure 4). While the inherent dielectric constant of a protein may indeed be lower than that of the surrounding solvent, the net effect is the same : the charges are screened effectively even at short distances (8−10 Å) unless they are well buried in the protein interior (Figure 4). The linear best fit of the internal protein dielectric experimental data in Figure 4 yields an $\epsilon_{prot}(r)$ of $3.8497r$. While this linear fitting approach is crude, it illustrates the large discrepancy between the commonly assumed ϵ_{prot} of 4 and actual solution state experimental results.

Despite this evidence from experiment, many theorists insist upon applying Ewald-derived methods designed for low-dielectric, crystal lattice applications to biomolecules in water, yet problems with this approach were reported more than 25 years ago for dipolar liquids (*7*, *33*, *34*). In particular, it was noted that the nonphysical behavior of Ewald methods allows arbitrary dipoles from the local unit cell to be grossly amplified by neighboring unit cells rather than being attenuated, as in the true case as well as when using spherical cutoffs.

There have now been many studies of water comparing cutoffs and Ewald summations. Independent of water force fields, computational protocols, and the software employed, Ewald summations lead to distortions in water structure and dynamics (*35*−*38*). To provide a comparison of cutoff methods and Ewald summations, results from a variety of recent studies are given in Table 2. Also in this table, we have used the reported diffusion constants to estimate the effective temperature of the solvent. The best agreement with experiment is from our F3C water model with proper cutoff treatment at an R_c of ≥8.0 Å.

Typically, when Ewald summation is applied to common water models, there tends to be a dramatic increase in the diffusion constant, away from the experimental value, reflecting an increase in temperature of 34−52 K. In the case of Mark and Nilsson's work (*35*), there was little or no change with respect to using a cutoff. Feller and co-workers (*36*) concluded that, "The diffusion constant calculated from the Ewald simulation is significantly further from experiment than the cutoff result, pointing out the need to reparametrize

Table 2: Effect of Long-Range Electrostatic Treatment on Bulk Water Self-Diffusion

ref[a]	water model	software	electrostatic treatment	cutoff[b] (Å)	T (K)	density (g/mL)	D (Å^2 ps^{-1})	effective T[c] (K)
1	experiment				298	0.997	0.23 ± 0.01	298
2	TIP3P model	CHARMM	shifted cutoff	12	293	0.999	0.39	322
2	TIP3P model	CHARMM	Ewald	12	293	0.999	0.51	336
3	SPC	DL_POLY	force shifted, eq 3	9	300	?	0.24	300
3	SPC	DL_POLY	Ewald	12	300	?	0.58	343
3	TIP3P	DL_POLY	force shifted, eq 3	9	300	?	0.39	322
3	TIP3P	DL_POLY	Ewald	12	300	?	0.63	349
4	TIP3P model	CHARMM	atom force shifted	8	298	0.998	0.57	343
4	TIP3P model	CHARMM	atom force shifted	12	298	0.998	0.58	344
4	TIP3P model	CHARMM	Ewald	12	298	0.998	0.56	342
5	TIP3P	BOSS	sharp truncation, eq 1	9	298	0.993	0.50	335
5	TIP4P	BOSS	sharp truncation, eq 1	9	298	0.990	0.33	314
5	TIP5P	BOSS	sharp truncation, eq 1	9	298	0.999	0.26	304
6	TIP4P-EW	?	Ewald	9.5	298	0.995	0.24	300
7	TIP5P-E	?	Ewald	9	298	1.000	0.28	307
8	F3C	ENCAD	atom force shifted	8	298	0.997	0.24	300
8	F3C	ENCAD	atom force shifted	10	298	0.997	0.23	298
8	F3C	ENCAD	atom force shifted	12	298	0.997	0.22	298
9	F3C	*il*mm	atom force shifted	8	298	0.997	0.23	298
9	F3C	*il*mm	atom force shifted	10	298	0.997	0.23	298
9	F3C	*il*mm	atom force shifted	12	298	0.997	0.22	298

[a] From ref *51* for 1, ref *36* for 2, ref *38* for 3, ref *35* for 4, ref *41* for 5, ref *39* for 6, ref *42* for 7, ref *18* for 8, and ref *37* for 9. [b] The cutoff for the Ewald simulations is for the real-space calculation. [c] Interpolation of temperature from experimental temperature vs water self-diffusion data of Krynicki et al. (*51*).

the TIP3P water model for use with Ewald summation", which has not been done to our knowledge.

Others have recognized the need to reparametrize other members of the TIP family of water models. Recently, both TIP4P and TIP5P (*39*−*41*), which are not routinely used in macromolecular simulations, have been "rehabilitated" for use exclusively with Ewald summation in treating the artifacts its use imposes on systems. The most promising of these is the TIP4P-EW work of Horn et al. (*39*) in which they tuned TIP4P, providing an improvement in the diffusion constant. However, reparametrization is not always the solution, as in the case of TIP5P-E (*42*), where the diffusion constant is perturbed away from both experiment and cutoff simulations.

In addition to an increase in the effective temperature with Ewald summation previously mentioned, there have been many studies showing that Ewald methods induce artificial periodicity in peptide and protein systems (*43*−*47*). These studies suggest that Ewald techniques yield unrealistically stable and inflexible peptides and proteins. Kastenholz and Hunenberger (*48*) concluded that, "artificial periodicity induces a nonnegligible energetical bias (and thus affects the sampling of solute configurations)." This artificial periodicity perturbs the potential of mean force for structural transitions, favoring those that are the most folded. These effects have been documented in CHARMM, AMBER, and GROMOS, all commonly used programs with different force fields. In our opinion, this bias alone makes Ewald methods inappropriate for studies of protein folding and/or unfolding.

The developers of one of the smooth particle mesh Ewald methods (*15*, *16*) identified a further problem related to robustness with PME. As a strict pairwise sum is not employed, it is not possible to achieve conservation of energy and linear momentum at the same time. This is a serious problem as we advocate the use of the NVE*p* ensemble. This ensemble requires rigorous treatment of the forces and the integration algorithm, resulting in a robust simulation environment with two independent checks on the stability of the numerical solutions (*1*, *7*).

A wide range of problems involving the use of Ewald summations in MD simulations have been documented: perturbation of water structure and dynamics, shifting conformational equilibria of peptides and proteins, failing to conserve both energy and linear momentum, and finally assuming, if not requiring, long-range ordering often inappropriate for solution simulations. Given these outstanding issues and the fact that spherical cutoff methods are significantly less computationally expensive than Ewald techniques for simulations of charged peptides and proteins, we prefer to model our solute in solvent without such imposed periodicity with a simple and efficient algorithm that enables access to simulation time scales typically unavailable to Ewald simulations. Finally, we have found that our force-shifted cutoff provides improved sampling of conformational space and much better agreement with experiment.

ACKNOWLEDGMENT

Some of the simulations presented were computed on hardware donated by Intel. Peptide structures in Figure 1 and 3 were created with MolScript (*49*) and rendered with Raster3D (*50*).

REFERENCES

1. Beck, D. A. C., and Daggett, V. (2004) Methods for Molecular Dynamics Simulations of Protein Folding/Unfolding in Solution, *Methods 34*, 112−120.
2. Loncharich, R. J., and Brooks, B. R. (1989) The Effects of Truncating Long-Range Forces on Protein Dynamics, *Proteins 6*, 32−45.
3. Brooks, C. L., Pettitt, B. M., and Karplus, M. (1985) Structural and Energetic Effects of Truncating Long Range Interactions in Ionic and Polar Fluids, *J. Chem. Phys. 83*, 5897−5908.
4. Schreiber, H., and Steinhauser, O. (1992) Cutoff size does strongly influence molecular dynamics results on solvated polypeptides, *Biochemistry 31*, 5856−5860.
5. Schreiber, H., and Steinhauser, O. (1992) Taming cut-off induced artifacts in molecular dynamics studies of solvated polypeptides. The reaction field method, *J. Mol. Biol. 228*, 909−923.
6. Schreiber, H., and Steinhauser, O. (1992) Molecular-Dynamics Studies of Solvated Polypeptides: Why the Cutoff Scheme Does Not Work, *Chem. Phys. 168*, 75−89.
7. Allen, M. P., and Tildesley, D. J. (1987) *Computer Simulation of Liquids*, Oxford University Press, Oxford, U.K.
8. Levitt, M., Hirshberg, M., Sharon, R., and Daggett, V. (1995) Potential-Energy Function and Parameters for Simulations of the Molecular-Dynamics of Proteins and Nucleic-Acids in Solution, *Comput. Phys. Commun. 91*, 215−231.
9. Steinbach, P. J., and Brooks, B. R. (1994) New Spherical-Cutoff Methods for Long-Range Forces in Macromolecular Simulation, *J. Comput. Chem. 15*, 667−683.
10. Daggett, V. (2000) Long time-scale simulations, *Curr. Opin. Struct. Biol. 10*, 160−164.
11. Padmanabhan, S., Marqusee, S., Ridgeway, T., Laue, T. M., and Baldwin, R. L. (1990) Relative Helix-Forming Tendencies of Nonpolar Amino Acids, *Nature 344*, 268−270.
12. Ewald, P. (1921) Die Berechnung optischer und elektrostatischer Gitterpotentiale, *Ann. Phys. 64*, 253−287.
13. Chakrabartty, A., Kortemme, T., Padmanabhan, S., and Baldwin, R. L. (1993) Aromatic Side-Chain Contribution to Far-Ultraviolet Circular-Dichroism of Helical Peptides and Its Effect on Measurement of Helix Propensities, *Biochemistry 32*, 5560−5565.
14. Brooks, B. R., Bruccoleri, R. E., Olafson, B. D., States, D. J., Swaminathan, S., and Karplus, M. (1983) CHARMM: A Program for Macromolecular Energy, Minimization, and Dynamics Calculations, *J. Comput. Chem. 4*, 187−217.
15. Essmann, U., Perera, L., Berkowitz, M. L., Darden, T., Lee, H., and Pedersen, L. G. (1995) A Smooth Particle Mesh Ewald Method, *J. Chem. Phys. 103*, 8577−8593.
16. Darden, T., York, D., and Pedersen, L. (1993) Particle Mesh Ewald: An N.Log(N) Method for Ewald Sums in Large Systems, *J. Chem. Phys. 98*, 10089−10092.
17. Taylor, D. L. (1982) Molecular-Dynamics of Actin In vitro and In vivo: A Fluorescence Approach, *Biophys. J. 37*, A89.
18. Levitt, M., Hirshberg, M., Sharon, R., Laidig, K. E., and Daggett, V. (1997) Calibration and testing of a water model for simulation of the molecular dynamics of proteins and nucleic acids in solution, *J. Phys. Chem. B 101*, 5051−5061.
19. Pardi, A., Billeter, M., and Wuthrich, K. (1984) Calibration of the Angular-Dependence of the Amide Proton-C-α Proton Coupling-Constants, $^3J_{HN\alpha}$, in a Globular Protein: Use of $^3J_{HN\alpha}$ for Identification of Helical Secondary Structure, *J. Mol. Biol. 180*, 741−751.
20. Scheraga, H. A., Vila, J. A., and Ripoll, D. R. (2002) Helix-coil transitions re-visited, *101*−*102*, 255−265.
21. Vila, J. A., Ripoll, D. R., and Scheraga, H. A. (2001) Influence of lysine content and pH on the stability of alanine-based copolypeptides, *58*, 235−246.
22. Harvey, S. C., Tan, R. K. Z., and Cheatham, T. E. (1998) The flying ice cube: Velocity rescaling in molecular dynamics leads to violation of energy equipartition, *J. Comput. Chem. 19*, 726−740.
23. Armen, R., Alonso, D. O. V., and Daggett, V. (2003) The role of α-, 3(10)-, and π-helix in helix → coil transitions, *Protein Sci. 12*, 1145−1157.
24. Wolf, D., Keblinski, P., Phillpot, S. R., and Eggebrecht, J. (1999) Exact method for the simulation of Coulombic systems by spherically truncated, pairwise r(−1) summation, *J. Chem. Phys. 110*, 8254−8282.
25. Conway, B. E., Bockris, J. O., and A., I. A. (1951) Dielectric constant of the solution in the diffuse and Helmholtz double layers

at a charged interface in aqueous solution, *Trans. Faraday Soc. 47*, 756−766.
26. Gilson, M. K., and Honig, B. H. (1986) The Dielectric Constant of a Folded Protein, *Biopolymers 25*, 2097−2119.
27. Rees, D. C. (1980) Experimental Evaluation of the Effective Dielectric Constant of Proteins, *J. Mol. Biol. 141*, 323−326.
28. Russell, A. J., Thomas, P. G., and Fersht, A. R. (1987) Electrostatic Effects on Modification of Charged Groups in the Active-Site Cleft of Subtilisin by Protein Engineering, *J. Mol. Biol. 193*, 803−813.
29. Russell, A. J., and Fersht, A. R. (1987) Rational Modification of Enzyme Catalysis by Engineering Surface Charge, *Nature 328*, 496−500.
30. Dwyer, J. J., Gittis, A. G., Karp, D. A., Lattman, E. E., Spencer, D. S., Stites, W. E., and Garcia-Moreno, B. (2000) High apparent dielectric constants in the interior of a protein reflect water penetration, *Biophys. J. 79*, 1610−1620.
31. Garcia-Moreno, B., Dwyer, J. J., Gittis, A. G., Lattman, E. E., Spencer, D. S., and Stites, W. E. (1997) Experimental measurement of the effective dielectric in the hydrophobic core of a protein, *Biophys. J. 64*, 211−224.
32. Rogers, N. K., Moore, G. R., and Sternberg, M. J. E. (1985) Electrostatic Interactions in Globular-Proteins: Calculation of the pH-Dependence of the Redox Potential of Cytochrome-C551, *J. Mol. Biol. 182*, 613−616.
33. Valleau, J. P., and Whittington, S. G. (1977) in *Statistical mechanics A. Modern theoretical chemistry* (Berne, B. J., Ed.) pp 140−162, Plenum, New York.
34. Adams, D. J., Adams, E. M., and Hills, G. J. (1979) Computer-Simulation of Polar Liquids, *Mol. Phys. 38*, 387−400.
35. Mark, P., and Nilsson, L. (2002) Structure and dynamics of liquid water with different long-range interaction truncation and temperature control methods in molecular dynamics simulations, *J. Comput. Chem. 23*, 1211−1219.
36. Feller, S. E., Pastor, R. W., Rojnuckarin, A., Bogusz, S., and Brooks, B. R. (1996) Effect of electrostatic force truncation on interfacial and transport properties of water, *J. Phys. Chem. 100*, 17011−17020.
37. Beck, D. A. C., Alonso, D. O., and Daggett, V. (2003) A microscopic view of peptide and protein solvation, *Biophys. Chem. 100*, 221−237.
38. Zahn, D., Schilling, B., and Kast, S. M. (2002) Enhancement of the wolf damped Coulomb potential: Static, dynamic, and dielectric properties of liquid water from molecular simulation, *J. Phys. Chem. B 106*, 10725−10732.
39. Horn, H. W., Swope, W. C., Pitera, J. W., Madura, J. D., Dick, T. J., Hura, G. L., and Head-Gordon, T. (2004) Development of an improved four-site water model for biomolecular simulations: TIP4P-Ew, *J. Chem. Phys. 120*, 9665−9678.
40. Mahoney, M. W., and Jorgensen, W. L. (2000) A five-site model for liquid water and the reproduction of the density anomaly by rigid, nonpolarizable potential functions, *J. Chem. Phys. 112*, 8910−8922.
41. Mahoney, M. W., and Jorgensen, W. L. (2001) Diffusion constant of the TIP5P model of liquid water, *J. Chem. Phys. 114*, 363−366.
42. Rick, S. W. (2004) A reoptimization of the five-site water potential (TIP5P) for use with Ewald sums, *J. Chem. Phys. 120*, 6085−6093.
43. Figueirido, F., DelBueno, G. S., and Levy, R. M. (1997) On finite-size corrections to the free energy of ionic hydration, *J. Phys. Chem. B 101*, 5622−5623.
44. Hummer, G., Pratt, L. R., Garcia, A. E., Berne, B. J., and Rick, S. W. (1997) Electrostatic potentials and free energies of solvation of polar and charged molecules, *J. Phys. Chem. B 101*, 3017−3020.
45. Weber, W., Hunenberger, P. H., and McCammon, J. A. (2000) Molecular dynamics simulations of a polyalanine octapeptide under Ewald boundary conditions: Influence of artificial periodicity on peptide conformation, *J. Phys. Chem. B 104*, 3668−3675.
46. Hunenberger, P. H., and McCammon, J. A. (1999) Effect of artificial periodicity in simulations of biomolecules under Ewald boundary conditions: A continuum electrostatics study, *Biophys. Chem. 78*, 69−88.
47. Hunenberger, P. H., and McCammon, J. A. (1999) Ewald artifacts in computer simulations of ionic solvation and ion−ion interaction: A continuum electrostatics study, *J. Chem. Phys. 110*, 1856−1872.
48. Kastenholz, M. A., and Hunenberger, P. H. (2004) Influence of artificial periodicity and ionic strength in molecular dynamics simulations of charged biomolecules employing lattice-sum methods, *J. Phys. Chem. B 108*, 774−788.
49. Kraulis, P. J. (1991) Molscript: A Program to Produce Both Detailed and Schematic Plots of Protein Structures, *J. Appl. Crystallogr. 24*, 946−950.
50. Merritt, E. A., and Bacon, D. J. (1997) Raster3D: Photorealistic molecular graphics, *Methods Enzymol. 277*, 505−524.
51. Krynicki, K., Green, C. D., and Sawyer, D. W. (1978) Pressure and temperature dependence of self-diffusion in water, *Disc. Faraday Soc. 66*, 199−208.

BI0486381